Supporting Information

Boosting photocatalytic H_2O_2 evolution through synergistic sulfur doping and crystalline engineering of carbon nitride

Yumeng Qi, Meiyu Xu, Shuting Deng, Bo Wang*, Shijie Wang*, Wei Zhou*

Shandong Provincial Key Laboratory of Molecular Engineering, School of Chemistry and Chemical Engineering, Qilu University of Technology (Shandong Academy of Sciences), Jinan, Shandong, 250353, P. R. China

**Corresponding authors. E-mail: wangb123@qlu.edu.cn (B. Wang), wsj0924@qlu.edu.cn (S. Wang), wzhou@qlu.edu.cn (W. Zhou)*

Experimental Section

Characterizations

The powder X-ray diffraction (XRD) patterns were tested using a Japanese Rigaku SmartLab SE X-ray diffractometer with a Cu Kα X-ray source (λ = 1.5406 Å). Transmission electron microscopy (TEM) was performed on a JEM-2100 instrument from Nippon Electronics Co., Ltd. Absorption spectra were performed on a UV-9000s UV-vis spectrometer from Shanghai Metash instruments Co., Ltd. The solid-state ^{13}C MAS NMR spectra were recorded on a Bruker 600 MHz solid-state NMR spectrometer at room temperature. The Fourier transform infrared (FTIR) spectra was carried out with a Bruker Tensor 27 Fourier infrared spectrometer from Germany. The specific surface area was determined from the adsorption branch of the N_2 adsorption-desorption isotherm using the Brunauer-Emmett-Teller (BET) equation. The corresponding pore size distribution was derived from the same adsorption branch data. The electron paramagnetic resonance (EPR) spectra were obtained on a Bruker EMX plus spectrometer at room temperature. The X-ray photoelectron spectroscopy (XPS) was tested using an ESCALAB Xi+ electron spectrometer from Thermo Fisher, which is equipped with a monochromatic Al Kα. The steady-state photoluminescence (PL) spectra and time-resolved photoluminescence (TRPL) spectra of the as-prepared samples were obtained using an Edinburgh FLS1000 fluorescence spectrometer. The diffuse reflectance spectrum (DRS) was recorded on a UV-vis-NIR spectrophotometer (Agilent Cary 2000) in the wavelength range of 200-800 nm. The steady-state surface photovoltage (SPV) measurement system includes computer, lock-in amplifier, monochromatic light and photovoltaic cell. The temperature-programmed oxygen desorption (O_2-TPD) measurements of the samples were performed using a Micromeritics Auto Chem II 2920 fully automated chemisorption analyzer.

Reactive species trapping experiments

Silver nitrate ($AgNO_3$), p-benzoquinone (pBQ), and β-carotene were employed as scavengers for electrons (e^-), superoxide radicals ($\cdot O_2^-$), and singlet oxygen ($^1O_2$), respectively. Aqueous solutions containing the corresponding scavenger (1 mM) were freshly prepared. In a typical experiment, 5 mg of the photocatalyst was dispersed in 20 mL of the scavenger-containing solution, consisting of 2 mL benzyl alcohol (10 vol%) and 18 mL of the 1 mM scavenger solution. The suspension was magnetically stirred in the dark for 30 min under continuous O_2 bubbling to establish adsorption-desorption equilibrium. The photocatalytic reactions were then carried out under the same conditions as described above. After 1 h of irradiation, 1.5 mL of the reaction solution was collected and filtered through a 0.22 μm membrane to remove the catalyst. The resulting clear supernatant was subsequently analyzed for H_2O_2 concentration. Control experiments without scavengers and with individual components were also conducted under identical conditions to ensure the reliability of the results.

H_2O_2 detection methods

The concentration of H_2O_2 was determined via an iodometric method. Briefly, 0.5 mL of potassium hydrogen phthalate ($KC_8H_5O_4$, 0.1 mol L^{-1}) and 0.5 mL of potassium iodide (KI, 0.4 mol L^{-1}) aqueous solutions were added to the collected supernatant. After standing for 30 min, H_2O_2 in the acidic medium (pH ≈ 3.5) oxidized iodide ions (I^-) to form triiodide ions (I_3^-), which exhibit a strong characteristic absorption peak around 350 nm. The absorbance at 350 nm was measured using a UV-Vis spectrophotometer.

Photochemical measurements

Photoelectrochemical performance testing was conducted on an electrochemical workstation (Shanghai Chenhua CHI760E). The test employed a three-electrode system: an Ag/AgCl electrode as the reference electrode, a platinum wire electrode as the counter electrode, and FTO conductive glass loaded with photocatalyst as the working electrode. Typically, 10.0 mg of catalyst is dispersed in a mixed solution consisting of 1.0 mL DMF and 20.0 µL naphthol. Ultrasonic treatment ensures thorough mixing, yielding a uniform suspension. Subsequently, 10.0 µL of the suspension is spotted onto a 0.5 cm × 0.5 cm area of the FTO glass surface and dried in a 60 °C oven to prepare the working electrode. A 300 W Xe lamp (PLS-FX300D, Beijing Perfect light Technology Co., Ltd.) was used as the light source with a 0.5 M Na_2SO_4 solution or a 10 mM mixture of $K_3Fe(CN)_6$ and $K_4FeC_6N_6{\bullet}3H_2O$ served as the electrolyte.

Rotating disk electrode (RDE) measurements

10.0 mg of the catalyst was dispersed in a mixed solution composed of 1.0 mL DMF and 20.0 µL Nafion. The mixture was then homogenized by ultrasonication to obtain a homogeneous catalyst suspension. Subsequently, 10.0 µL of the suspension was drop-cast onto the surface of a glassy carbon rotating disk electrode (RDE, 0.196 cm^2) and dried naturally in ambient air to fabricate the working electrode. An Ag/AgCl electrode and a carbon rod were employed as the reference electrode and the counter electrode, respectively.

Linear sweep voltammetry was performed in an O_2-saturated phosphate buffer solution (pH = 7) at a scan rate of 5 mV s^{-1}. The average electron transfer number (n) for the oxygen reduction reaction was calculated from the slopes of the corresponding Koutecky-Levich plots using the following equation:

$$J^{-1} = J_k^{-1} + B^{-1}\omega^{-\frac{1}{2}}$$

$$B = 0.2nFC_0D_0^{\frac{2}{3}}\nu^{-\frac{1}{6}}$$

where J, J_k, and ω are the measured current density, kinetic limiting current density and rotating rate (rpm), respectively. In addition, B is determined from the slope of the Koutecky-Levich plots, and F is the Faraday constant (F = 96485 C mol^{-1}). Moreover, C_0 is the concentration of O_2 in the solution ($C_0 = 1.26\times10^{-6}$ mol cm^{-3}), D_0 is the diffusion coefficient of O_2 ($D_0 = 2.7\times10^{-5}$ cm^2 s^{-1}), and v is the kinematics viscosity of the electrolyte (v = 0.01 cm^2 s^{-1}).

In-situ DRIFTS testing experiments

In-situ Fourier transform infrared spectra (in-situ FTIRS) were recorded using a Bruker Tensor 27 spectrometer. The CSCN powder was loaded into an in-situ sample cell and purged with N_2 flow for 30 min to remove residual gases before collecting the background spectrum. Subsequently, the atmosphere was switched to a continuous flow of a mixture of O_2 and water vapor for 30 min, during which IR spectra were collected at 10-min intervals. A 300 W xenon lamp (PLS-FX300D, Beijing Perfect light Technology Co., Ltd.) was employed as the light source throughout the experiments.

The apparent quantum yield (AQY) measurement

The apparent quantum yield (AQY) for H_2O_2 production was determined under monochromatic light irradiation using a bandpass filter (365 nm, 385 nm, 420 nm, 450nm, 485nm and 520 nm). The effective irradiation area was approximately 7.065 cm^2.

The amount of H_2O_2 generated during 1 h of photocatalytic reaction was quantified, and the AQY was calculated according to the following equation:

$$AQY(\%) = \frac{2 * number\ of\ H_2O_2\ molecules\ formed}{number\ of\ incident\ photons} * 100\%$$

$$= \frac{2 * M(H_2O_2) * N_A * h * c}{S * P * t * \lambda} * 100\%$$

Where $M(H_2O_2)$ is the amount of produced H_2O_2 (mol), N_A is Avogadro's constant (6.02×10^{23} mol^{-1}), h is Planck's constant (6.626×10^{-34} J·s), c is the speed of light (3.0×10^8 m·s^{-1}), S is the irradiation area (7.065 cm^2), P is the incident light intensity at 420 nm (0.0485 W·cm^{-2}), t is the irradiation time (3600 s), and λ is the wavelength of the incident light (420 × 10^{-9} m).

DFT calculations

All calculations were carried out for the material in the framework of Density Functional Theory (DFT) using the Vienna Ab initio Simulation Package (VASP 6.3.0).[1, 2] The generalised gradient approximation (GGA) of the Perdew-Burke-Ernzerhof (PBE) function was used to describe the exchange-correlation energy.[3] The projected augmented wave (PAW) method and pseudopotentials were used to describe the interactions between valence electrons and ions.[4]

To ensure the efficiency of the computational results and parallel computing. A 3*3*1 k-point grid under Monkhorst-Pack is used in the optimisation process and 450 eV truncation energy is set. The lattice parameters and ionic positions of all crystals were fully relaxed, and the convergence criteria for the total energy of all relaxed atoms and the final force were 10^{-6} eV and 0.03 eV/Å, respectively.

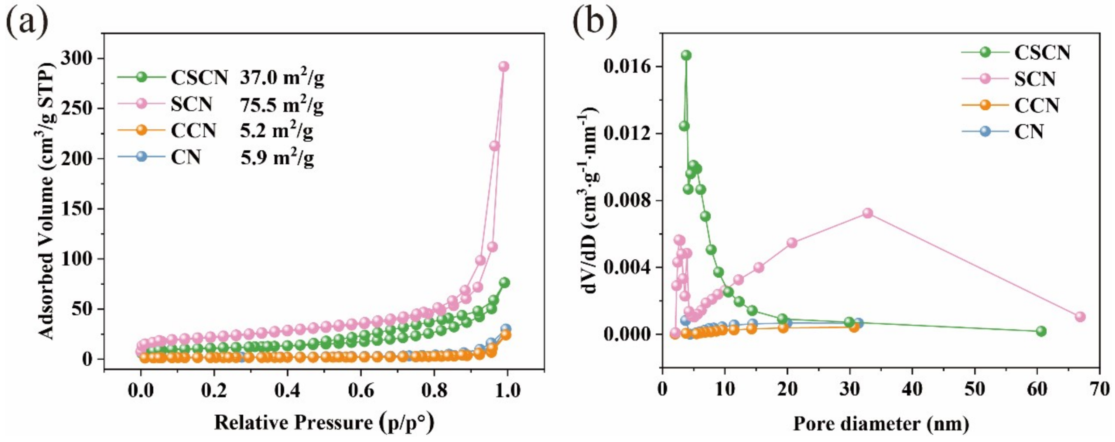

Fig. S1. (a) N_2 adsorption-desorption isotherms and (b) the corresponding pore size distributions for CN, SCN, CCN, and CSCN.

Table S1. The elemental composition (C, N, H, and S content) quantified using elemental analysis (EA).

	N (%)	C (%)	H (%)	S (%)
CN	62.06	35.16	1.965	-
CCN	53.60	31.19	1.639	-
SCN	61.52	35.25	1.768	0.154
CSCN	44.34	27.08	2.244	0.105

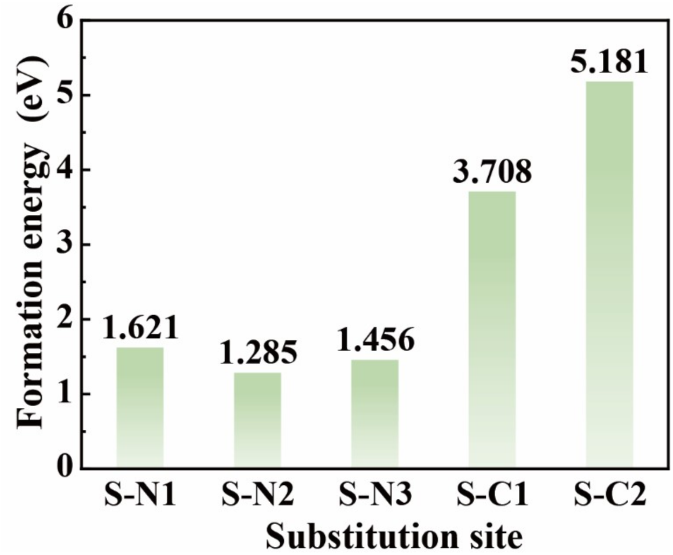

Fig. S2. Formation energies for S substitution at different C/N atomic sites.

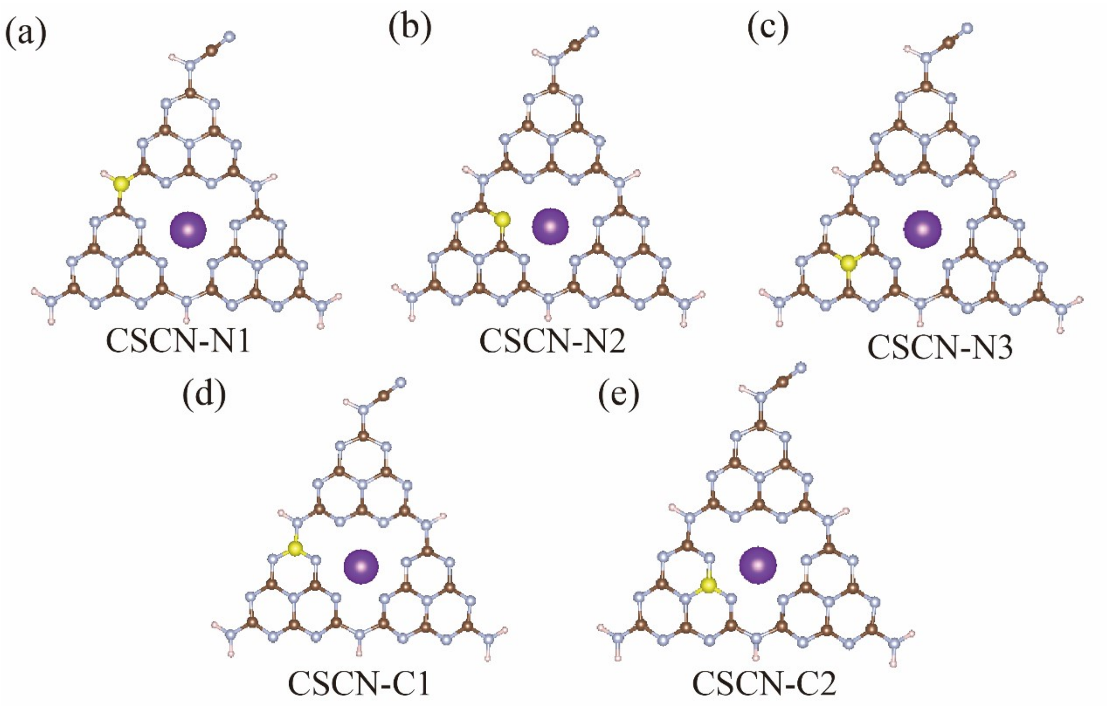

Fig. S3. Structural models for S substitution at different C/N atomic sites.

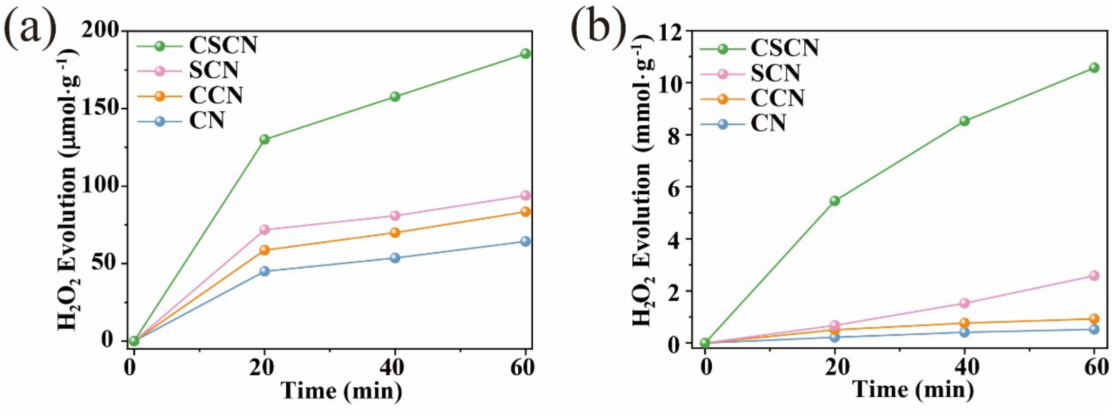

Fig. S4. Photocatalytic activity of CN, CCN, SCN and CSCN for H_2O_2 generation in (a) pure water and (b) 10% (v/v) benzyl alcohol.

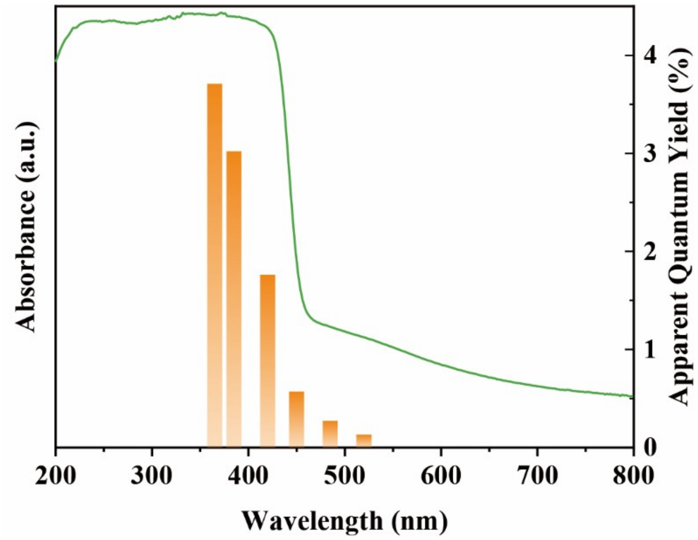

Fig. S5. Apparent quantum yield (AQY) of CSCN as a function of irradiation wavelength.

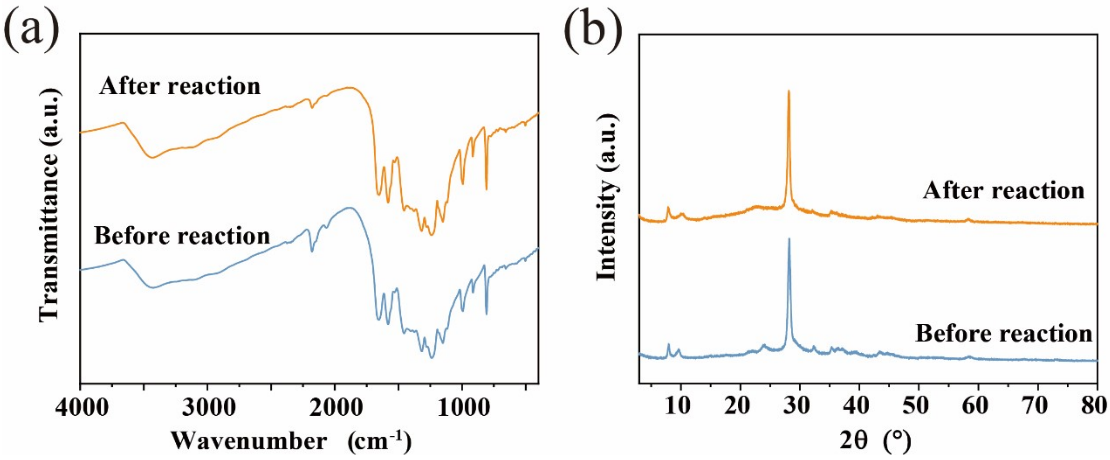

Fig. S6. (a) FTIR spectra and (b) XRD patterns of CSCN before and after the photocatalytic H_2O_2 production reaction.

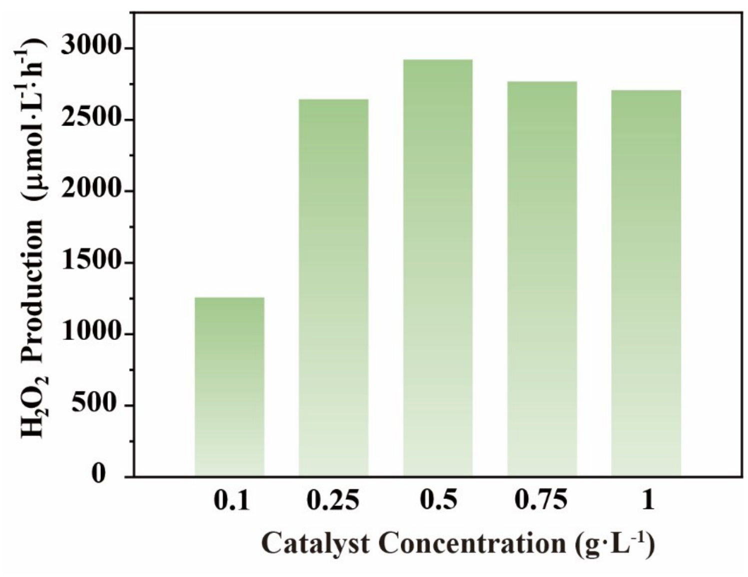

Fig. S7. Effect of catalyst concentrations on photocatalytic H_2O_2 production (0.1-1 g·L^{-1}).

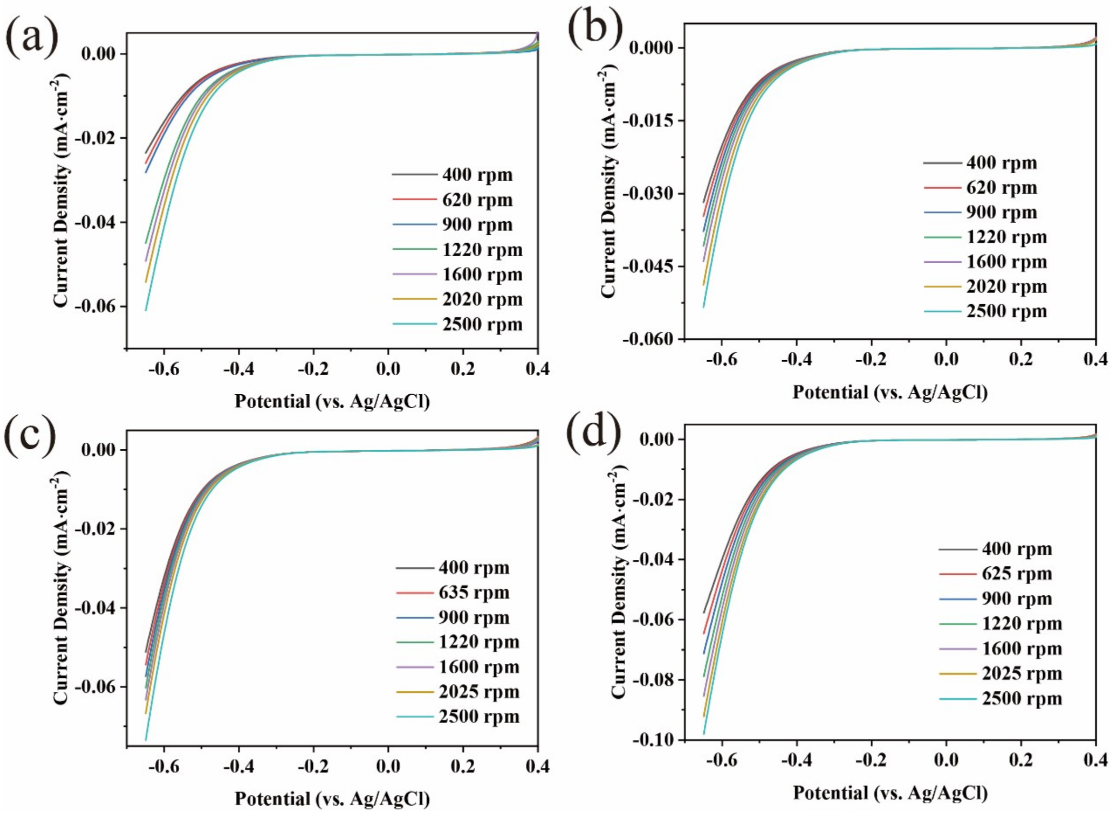

Fig. S8. LSV curves of (a) CN, (b) CCN, (c) SCN, and (d) CSCN recorded at various electrode rotation speeds.

Table S2. Exponential decay fitting parameters of fluorescence lifetime for experimental samples.

Sample	τ_1/ns	A_1	τ_2/ns	A_2	τ_{ave}/ns
CN	1.12675	0.69017	4.88278	0.38321	3.78
CCN	1.36687	0.9448	6.40376	0.14393	3.64
SCN	1.21653	0.88777	5.85387	0.20996	3.68
CSCN	0.67634	1.17037	5.62834	0.03436	1.65

The time-resolved PL spectra were fitted with a biexponential decay function, and the average PL lifetime (τ_{ave}) was calculated using the equation below:

$$\tau_{ave} = \frac{A_1 \times \tau_1^2 + A_2 \times \tau_2^2}{A_1 \times \tau_1 + A_2 \times \tau_2}$$

τ_i is the estimated lifetime value and A_i is the corresponding amplitude.

Table S3. Comparison of H_2O_2 production activity in O_2-saturated pure water with reported systems.

Photocatalyst	Catalyst Concentration (g L^{-1})	Light source	H_2O_2 production (mmol g^{-1} h^{-1})	Refs
g-C_3N_4-Au	0.5	300 W Xe lamp (AM 1.5)	16.14	5
g-C_3N_4/PDI BNrGO	1.67	300 W Xe lamp (λ ≥ 420 nm)	29.1	6
C_3N_4-nv	1.0	300 W Xe lamp (λ ≥ 420 nm)	75.66	7
CNTTT-CTF	0.5	LED lamp (λ ≥ 400 nm)	96	8
OCN-500	1.0	300 W Xe lamp (λ ≥ 420 nm)	106	9
ZnPPc-NBCN	0.5	100 mW/cm^2 Xe lamp (λ ≥ 400 nm)	114	10
HJ-C_3N_4	1.0	300 W Xe lamp (λ ≥ 400 nm)	115	11
CO/AQ/C_3N_4	0.5	300 W Xe lamp (AM 1.5 G)	124	12
Nv-C≡N-CN	1.0	300 W Xe lamp (λ ≥ 420 nm)	137	13
CN-NH_4-NaK	0.5	300 W Xe lamp (λ ≥ 420 nm)	139	14
CSCN	**0.25**	**450 mW/cm^2 LED lamp (780 nm ≥ λ ≥ 380 nm)**	**185.41**	**This work**

Table S4. Comparison of photocatalytic H_2O_2 production in sacrificial agent-containing, O_2-saturated aqueous systems with recent reports.

Photocatalyst	Sacrificial agent	Catalyst Concentration (g L^{-1})	Light source	H_2O_2 production (mmol g^{-1} h^{-1})	Refs
UCN4	10 vol.% EtOH	1.0	300 W Xe lamp (λ ≥ 420 nm)	99.11	15
CN/HMoP	5 vol.% EtOH	0.5	300 W Xe lamp (λ ≥ 420 nm)	226.2	16
BI-CN3	10 vol.% EtOH	0.5	5 W LED lamp (λ ≥ 420 nm)	706	17
DDCN	10 vol.% MtOH	0.2	300 W Xe lamp (λ ≥ 420 nm)	1031	18
C-P-CN	10 vol.% EtOH	1.0	300 W Xe lamp (λ ≥ 400 nm)	3320	19
Cv@g-C_3N_4	10 vol.% EtOH	1.0	300 W Xe lamp (λ ≥ 420 nm)	7010	20
Sb_1/Cv-C_3N_4	10 vol.% IPA	1.0	300 W Xe lamp (λ ≥ 400 nm)	5369	21
Ag@T-C_3N_4	50 vol.% BA	1.0	300 W Xe lamp (λ ≥ 420 nm)	4729.82	22
TP-PCN	10 vol.% IPA	0.5	300 W Xe lamp (λ ≥ 420 nm)	6530.8	23
CCN-550	1 vol.% BA	1.33	300 W Xe lamp (λ ≥ 420 nm)	4379.18	24
CSCN	**10 vol.% BA**	**0.25**	**450 mW/cm^2 LED lamp (780 nm ≥ λ ≥ 380 nm)**	**11840**	**This work**

Table S5. Comparative assessment of representative H_2O_2 production routes.

Method	Reaction Pathway	Advantages	Limitations	Applicable Scale	Refs
Anthraquinone Process	Hydrogenation-oxidation cycle using anthraquinone carriers	High productivity; well-established industrial infrastructure	Relies on organic solvents and Pd-based catalysts; waste generation and environmental concerns	Large-scale industrial	25
Direct Synthesis ($H_2 + O_2$)	Catalytic combination of Hydrogen and Oxygen to form H_2O_2	High atom economy; relatively straightforward reaction pathway	Safety risks (explosive gas mixtures); high equipment requirement.; requires noble metal catalysts	Medium-small scale production	26
Electrochemical Method	Two-electron oxygen reduction reaction ($2e^-$ ORR) at the cathode	Environmentally friendly, suitable for small-scale production.	High electricity consumption; low efficiency	Small-scale production	27
Photocatalytic Method	Light-driven reduction of O_2 in aqueous systems using semiconductor photocatalysts	Utilizes solar energy; mild conditions; no hazardous reagents; compatible with pure water systems	Current efficiency and stability need improvement; relatively low reaction rate compared to industrial routes	Suitable for sustainable production	28

References

1. G. Kresse, J. Furthmüller, *Phy. Rev. B.,* 1996, **54**, 11169-11186.
2. G. Kresse, D. Joubert, *Phy. Rev. B.,* 1999, **59** 1758-1775.
3. J.P. Perdew, K. Burke, M. Ernzerhof, *Phys. Rev. Lett.,* 1996, **77**, 3865-3868.
4. P.E. Blöchl, Projector augmented-wave method, *Phy. Rev. B.,* 1994, **50**, 953-17979.
5. G. Wang, T. Huang, Y. Tan, S. Liu, R. Wu, Z. Fang, B. Yang, S. Wei, *ACS Appl. Nano Mater.,* 2025, **8**, 6125-6132.
6. Y. Kofuji, Y. Isobe, Y. Shiraishi, H. Sakamoto, S. Tanaka, S. Ichikawa, T. Hirai, *J. Am. Chem. Soc.,* 2016, **138**, 10019-10025.
7. Y. Lu, Y. Guo, S. Zhang, L. Li, R. Jiang, D. Zhang, J.C. Yu, J. Wang, *ACS Nano,* 2024, **18**, 20435-20448.
8. P. Shang, X. Yang, X. Zou, Y. Li, S. Pang, *Commun. Mater.,* 2025, **6**, 102.
9. Z. Wei, M. Liu, Z. Zhang, W. Yao, H. Tan, Y. Zhu, *Energy Environ. Sci.,* 2018, **11**, 2581-2589.
10. Y.-X. Ye, J. Pan, F. Xie, L. Gong, S. Huang, Z. Ke, F. Zhu, J. Xu, G. Ouyang, *Proc. Natl. Acad. Sci.,* 2021, **118**, e2103964118.
11. P. Ma, X. Zhang, C. Wang, Z. Wang, K. Wang, Y. Feng, J. Wang, Y. Zhai, J. Deng, L. Wang, K. Zheng, *Appl. Catal. B-Environ.,* 2022, **300**, 120736.
12. C. Chu, Q. Zhu, Z. Pan, S. Gupta, D. Huang, Y. Du, S. Weon, Y. Wu, C. Muhich, E. Stavitski, K. Domen, J.-H. Kim, *Proc. Natl. Acad. Sci.,* 2020, **117**, 6376-6382.
13. X. Zhang, P. Ma, C. Wang, L. Gan, X. Chen, P. Zhang, Y. Wang, H. Li, L. Wang, X. Zhou, K. Zheng, *Energy Environ. Sci.,* 2022, **15**, 830-842.
14. F. He, Y. Lu, Y. Wu, S. Wang, Y. Zhang, P. Dong, Y. Wang, C. Zhao, S. Wang, J. Zhang, S. Wang, *Adv. Mater.,* 2024, **36** 2307490.
15. C. Zhou, Y. Song, Z. Wang, J. Liu, P. Sun, Z. Mo, J. Yi, L. Zhai, *J. Environ. Chem. Eng.,* 2023, **11**, 110138.
16. X. Liu, Y. Li, K. Lin, Y. Jiang, *J. Colloid Interface Sci.,* 2024, **654**, 1228-1239.
17. A. Meng, X. Ma, D. Wen, W. Zhong, S. Zhou, Y. Su, *Chin. J. Catal.,* 2024, **60**, 231-241.
18. G. Ba, H. Hu, F. Bi, J. Yu, E. Liu, J. Ye, D. Wang, *Appl. Catal., B-Environ.,* 2025, **361**, 124645.
19. W. Wei, L. Zou, J. Li, F. Hou, Z. Sheng, Y. Li, Z. Guo, A. Wei, *J. Colloid Interface Sci.,* 2023, **636**, 537-548.
20. L. Chen, C. Chen, Z. Yang, S. Li, C. Chu, B. Chen, *Adv. Funct. Mater.,* 2021, **31**, 2105731.
21. Q. He, J. Ding, H.-J. Tsai, Y. Liu, M. Wei, Q. Zhang, Z. Wei, Z. Chen, J. Huang, S.-F. Hung, H. Yang, Y. Zhai, *J. Colloid Interface Sci.,* 2023, **651**, 18-26.
22. X. Zhou, K. Cao, S. Huang, H. Wu, Z. Cao, H. Liu, P. Chen, D. Su, G. Wang, T. Wang, C. Wang, H. Pang, *Angew. Chem. Int. Ed.,* 2025, **137**, e202505532.
23. H. Che, X. Gao, J. Chen, J. Hou, Y. Ao, *Angew. Chem. Int. Ed.,* 2021, **60**, 25546-25550.
24. J.J. Foo, S.-F. Ng, S.H. Kok, X. Zeng, L.-L. Tan, W.-J. Ong, *Chem. Eng. J.,* 2025, **505**, 158992.
25. H. B. Li, B. Zheng, Z. Y. Pan, B. N. Zong and M. H. Qiao, Front. Chem. Sci. Eng., 2018, **12**, 124-131.
26. Y. Zhang, X. L. Wang, Z. Y. Wang, L. Y. Liu, X. H. He and H. B. Ji, Dalton Trans., 2024, **53**, 18069-18082.
27. Y. N. Wang, J. T. Wu, Q. Zhang, Y. J. Tan, J. Gao, X. D. Zhu, Y. C. Zhang and S. J. Guo, Matter, 2025, **8**, 11.
28. Y. Y. Tang, W. M. Wang, J. Q. Ran, C. Peng, Z. X. Xu and W. H. Chu, Energy Environ. Sci., 2024, **17**, 6482-6498.